

## Large deviation spectrum estimation in two dimensions

Mohamed Abadi <sup>1</sup>, and Enguerran Grandchamp <sup>1</sup>

GRIMAAG UAG, Campus de Fouillole, French West Indies University,  
97157 Pointe-à-Pitre Cedex Guadeloupe France  
{mabadi, egrandch}@univ-ag.fr

**Abstract.** This paper deals with image processing. This study takes place in a segmentation process based on texture analysis. We use the multifractal approach to characterize the textures. More precisely we study a particular multifractal spectrum called the large deviation spectrum. We consider two statistical methods to numerically compute this spectrum. The resulting spectrum, computed by both methods over an image, is a one dimension spectrum. In the scope of this article, we extend these methods in order to obtain a two dimensions spectrum which could be assimilated to an image. This 2D spectrum allows a local characterization of the image singularities while a 1D spectrum is a global characterization. Moreover, the computation of the spectrum requires the use of a measure. We introduce here a pre processing based on the gradient to improve the measure. We show results on both synthetic and real world images. Finally, we remark that the resulting 2D spectrum is close to the resulting image of an edge detection process while edge detection using one dimension spectrum requires post processing methods. This statement will be used for future works.

**Keywords.** multifractal analysis, multifractal spectrum, numerical computing spectrum, Hölder exponent, Choquet capacity,

### 1 Introduction

Texture analysis techniques have been intensively studied over the last decades, among and the image processing community. Within these techniques, multifractal analysis was introduced by Parisi and Frisch [3] to study the singularities of 1d-signals and has yielded some interesting results. Nevertheless, as many tools of multifractal analysis have been developed initially for 1d-signals, there is no direct way to use them on images without losing the intrinsic 2d-relation between two neighbour pixels. For example, [14] used the large deviation spectrum to detect edges in images. However, in this study, the computation of the large deviation spectrum considers the image as a 1d-signal.

This article deals with the generalisation of large deviation spectrums to the case of 2d-signals. In order to do so, we will reconsider many approaches from the 1d-case. All of these approaches deal with a so-called multifractal spectrum which is roughly a tool used to quantify the number of points having the same Hölder exponent (singularity). As the estimation of this number of points is particularly difficult when dealing with discrete data, many numerical approaches can be found in the literature.

The original study [3] was based on the study of the power law behaviour in structure functions [4, 5]. As the computation used the Legendre transform, the estimated multifractal spectrum was called “Legendre Spectrum”. However, as shown by Muzy and al. [6], Arneodo and al. [7], the structure function method has many drawbacks. Particularly, it does not allow to access to the whole spectrum. They both present a new method to apply a multifractal analysis based on a wavelet transform modulus maxima [8, 9, 10] still conducting to a Legendre spectrum estimation.

Other authors suggest applying the multifractal analysis on a measure defined over the signal itself. Turiel and al [11, 12] compute fractal sets and are particularly interested on the MSM (Most Singular Manifold) set. MSM allows to characterize a signal from a geometrical and statistical point of view applying the gradient operator over the initial signal and then using a wavelet transform in order to determine the fractal sets.

Lévy-Véhel and al. [13] use the Choquet capacity firstly to define measures, secondly to determine the Hölder exponents and then to compute the multifractal spectrum. In this way, they introduce the kernel method and the histogram method to estimate, in a one dimension context, a multifractal spectrum called the “large deviation spectrum” [1]. This spectrum allows to characterize the singularities in a statistical way.

This last approach, as previously said, was applied successfully in [14] to an application of edge detection and is the one we would like to generalise.

The article is built as follow. After having presented some mathematical pre-requisite and the way to compute the singularity exponents and 1d large deviation spectrum (section 2) we will focus on the 2d case (section 3) in which the resulting spectrum is an image. As the spectrum computation depends on the definition of a measure, we will test two of them. The first uses the Choquet capacity as in [13, 16] and we will introduce a second measure based on the combination of the gradient and Choquet capacity. A comparison between the results obtained with each measure will be made in section 4. Section 5 is dedicated to conclude the article.

## **2 Multifractal formalism**

We present in this section the formalism used to compute the multifractal large deviation spectrum. We use the following steps:

1. Image normalization,
2. Multifractal measure defined by the Choquet Capacity [13],
3. Hölder exponents computation,
4. Spectrum computation.

### 2.1. Singularities computation

Let  $\mu$  be a measure defined over a set  $E \in [0,1[ \times [0,1[$ ,  $P(E)$  is a partition sequence of  $E$  and  $\nu_n$  is an increasing sequence of positive integer.

In this case, the partitions are defined as follow:

$$E_{i,j,n} = \left\{ \left[ \frac{i}{\nu_n}, \frac{i+1}{\nu_n} \right] \times \left[ \frac{j}{\nu_n}, \frac{j+1}{\nu_n} \right] \right\}$$

For image analysis applications, we choose that the set  $E_{i,j,n}$  is a window of size  $n$  centred on the point of coordinates  $(i, j)$ , i.e.  $|E_{i,j,n}| = n$ . This window is slide over the whole image by moving the center to its neighbours. In other words, the centre of the new set  $E_{i',j',n}$  will have the coordinates  $(i', j') = (i+1, j+1)$  if the movement is over the image diagonal,  $(i', j') = (i, j+1)$  for a horizontal one and  $(i', j') = (i+1, j)$  for a vertical one.

Then for each image point  $(i, j)$  singularities exponents are given by the Hölder exponents.

$$\alpha(x, y) = \lim_{r \rightarrow \infty} \frac{\log[\mu(B_r(x, y))]}{\log(r)}$$

Where  $B_r(x, y)$  is a window of size  $r = 2m + 1$  with  $m = 0, 1, \dots, \left\lfloor \frac{n}{2} \right\rfloor$  and  $(x, y) = (1, \dots, r)^2$ .  $|E_{i,j,n}|$  is the size of the partition of  $E$  and  $\mu$  the measure defined by the Choquet capacity on each window. Table 1. shows a representation of an image and three windows, respectively of size  $r = \{1, 3, 5\}$ .

In practice  $\alpha(x, y)$  is determinate by the slope of the linear regression of the following log curve:  $\log[\mu(B_r(x, y))]$  versus  $\log(r)$ . The Figure 1. shows the projection of the measure, built in Table 2. with a sum operator capacity, over the logarithmic scale and also the singularity computation using the slope of the linear regression ( $\alpha(i, j) = 2.288$ ). This allows to characterize the behaviour of the measure  $\mu$  at the neighbourhood of  $(x, y)$ .

64	63	54	47	50	54	61	71
64	61	51	48	55	61	64	70
58	54	46	47	59	65	65	67
46	45	42	46	58	63	62	63
37	42	45	49	58	61	60	63
37	46	52	57	63	62	61	66
41	50	57	62	68	66	63	66
44	52	57	62	70	68	63	63

$(i, j)$

$r = \{1,3,5\}$

**Table 1.** Matrix representing the image and three windows respectively of size  $r = \{1,3,5\}$

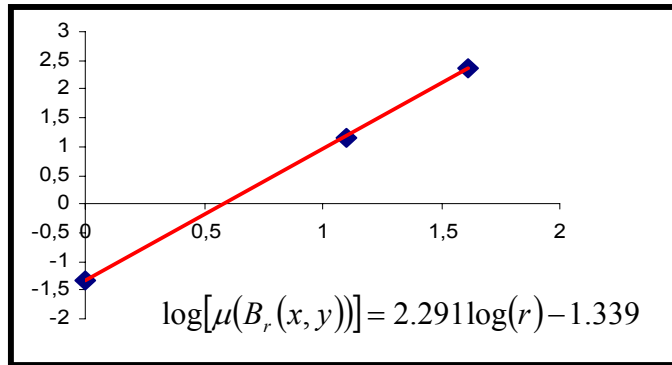


**Figure 1.** Linear regression on a logarithmic scale

0	0	0	0	0	0	0	0
0	0	0	0	0	0	0	0
0	0	2.291	2.284	1.867	1.846	0	0
0	0	2.613	2.368	1.934	1.919	0	0
0	0	2.311	2.232	1.983	1.995	0	0
0	0	1.971	1.972	1.899	1.996	0	0
0	0	0	0	0	0	0	0
0	0	0	0	0	0	0	0

**Table 2.** Hölder coefficients after image normalization with  $r = \{1,3,5\}$  and

$$n = |E_{i,j,n}| = 5$$

For image processing applications, the multifractal analysis is based on the estimation of the multifractal spectrum determined by the Hausdorff dimension [17], the Legendre spectrum [13] or the large deviation spectrum [1]. In the scope of this article we study the last spectrum.

The main idea is to use a sequence of Choquet capacities which allows the extraction of local and global information from the image in order to study the singularity behaviour.

## 2.2. Choquet capacity measure

In this section,  $\mu$  is a measure defined by the Choquet capacity. In the literature we found many capacities [14, 15] with a general definition having the following shape:

$$\mu(x, y) = O(i, j)_{\in B_r(x, y)} g(i, j)$$

With  $O$  an operator dealing with the intensity of a pixel  $g(i, j)$ . As examples, we can cite: the sum operator  $O = \sum$ , which is not a real informative measure of the image since it computes the sum of the intensities within a window, the maximum and minimum operator respectively  $O = \max$  and  $O = \min$ , which have a low sensibility to the singularity amplitude. Other operators have been introduced like self-similar or iso operator, more details are given respectively in [16] and [13].

The main drawback of these operators is their lack of sensibility to the amplitude or to the spatial distribution of the singularities.

In this article, our gait takes as a starting point the work carried out by Turiel and al. [11] to determine the fractals sets. We combine one of the previous operators with the gradient  $\nabla$  computed on each pixel, defined over two axes, and the norm. Thus we obtain three measures which are sensible simultaneously to amplitude and spatial distribution of the singularities. These measures have the following expression

$$\begin{aligned}\mu_x(x, y) &= O \nabla_x g(x, y) \\ \mu_y(x, y) &= O \nabla_y g(x, y) \\ \mu_{xy}(x, y) &= \sqrt{[\mu_x(x, y)]^2 + [\mu_y(x, y)]^2}\end{aligned}$$

Using these measures we can compute the singularity coefficients along the two axes and also that the norm. In this paper, we use, in particular, the gradient norm because it allows a correct representation and describe the brusque variations of images intensity:

$$\begin{aligned}\alpha_x(x, y) &= \lim_{r \rightarrow \infty} \frac{\log[\mu_x(B_r(x, y))]}{\log(r)} \\ \alpha_y(x, y) &= \lim_{r \rightarrow \infty} \frac{\log[\mu_y(B_r(x, y))]}{\log(r)}\end{aligned}$$

$$\alpha_{xy}(x, y) = \lim_{r \rightarrow \infty} \frac{\log[\mu_{xy}(B_r(x, y))]}{\log(r)}$$

After the computation of the Hölder exponents, we can focus on the multifractal spectrum estimation. In the following of the article, we will study the definition and the method to compute the large deviation spectrum.

### 3. Numerical estimation of the large deviation spectrum

Let us introduce in this section a two dimension adaptation of the two methods defined by Lévy Véhel and al. [1]. This adaptation allows estimating the large deviation spectrum from a measure construct by a combination between the previous operators and the gradient computed on both axes and previously describing.

This is a way to characterize the singularities and to study their behaviour in a statistical point of view. In the two dimension case, we define the large deviation spectrum as follow:

$$f_g[\alpha(i, j)] = \lim_{r \rightarrow \infty} \frac{\log[N_r(\alpha(i, j))]}{\log(r)} \quad (M1)$$

$$f_g^\varepsilon[\alpha(i, j)] = \lim_{\varepsilon \rightarrow 0} \lim_{r \rightarrow \infty} \frac{\log[N_r^\varepsilon(\alpha(i, j))]}{\log(r)} \quad (M2)$$

where  $N_r[\alpha(i, j)] = \#\{ \alpha(x, y) / \alpha(i, j) = \alpha(B_r(x, y)) \}$  for the first method and  $N_r^\varepsilon[\alpha(i, j)] = \#\{ \alpha(x, y) / \alpha(B_r(x, y)) \in [\alpha(i, j) - \varepsilon, \alpha(i, j) + \varepsilon] \}$  for the second one, which is a variant.  $\alpha(i, j)$  is the singularity in the centre of the window  $B_r$  of size  $r$ ,  $\alpha(x, y)$  is the singularity within  $B_r$  at the spatial coordinates  $(x, y)$ .

The first estimation using (M1) allows to compute the number  $N_r[\alpha(i, j)]$  of singularities  $\alpha(i, j)$  equals to  $\alpha(B_r(x, y))$ . For the second estimation (M2),  $N_r^\varepsilon[\alpha(i, j)]$  represent the number of  $\alpha(x, y)$  that belong to the interval  $[\alpha(i, j) - \varepsilon, \alpha(i, j) + \varepsilon]$ .

For image processing purpose, both methods are summarized with the following algorithm:

for each pixel  $(i, j)$ ,

for  $m = 0$  to  $m = |E_{i,j,n}|$

$$r = 2m + 1$$

compute  $N_r[\alpha(i, j)]$  (resp.  $N_r^\varepsilon[\alpha(i, j)]$ )

There is three particular values of  $m$

$m = 0 \Rightarrow r = 1 \Leftrightarrow B_{r=1} = 1$  pixel  $\Leftrightarrow (x, y) = (i, j)$  (minimal window size)

$m \neq 0$  and  $m \neq |E_{i,j,n}| \Leftrightarrow B_r$  is a window of size  $r \times r \Leftrightarrow (x, y) \in \{1, 2, \dots, r\}^2$

$m = |E_{i,j,n}| \Leftrightarrow B_r$  is a window of size  $|E_{i,j,n}| \times |E_{i,j,n}|$  where  $(x, y) \in \{1, 2, \dots, |E_{i,j,n}|\}^2$  (maximum window size)

The spectrum will be estimated by the slope of the linear regression  $\log[N_r(\alpha(i, j))]$  versus  $\log(r)$ . Table 3. illustrates the Hölder exponents and three windows used to compute the number of singularities  $N_r(\alpha(i, j))$  centred on  $(i, j)$ . Figure 2. shows the projection over the logarithmic scale and the linear regression for both methods and also the computation of the large deviation spectrums  $f_g$  et  $f_g^\varepsilon$ .

Then Table 4. shows the large deviation spectrum matrices for both methods.

0	0		0	0	0	0	0
0	0	0	0	0	0	0	0
0	0	2.291	2.284	1.867	1.846	0	0
0	0	2.613	2.368	1.934	1.919	0	0
0	0	2.311	2.232	1.983	1.995	0	0
0	0	1.971	1.972	1.899	1.996	0	0
0	0	0	0	0	0	0	0
0	0	0	0	0	0	0	0

**Table 3.** Hölder exponents and windows of size  $r = \{1, 3, 5\}$

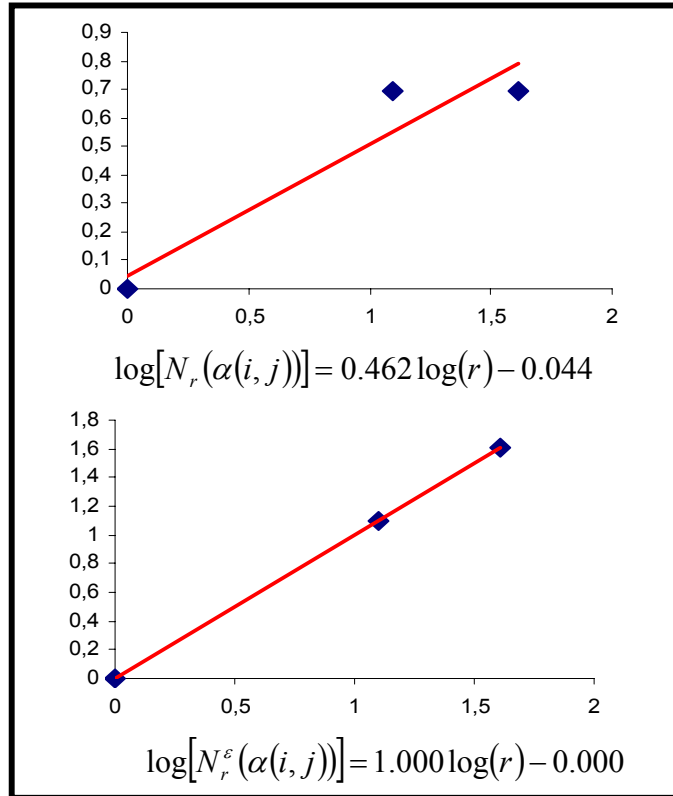


**Figure 2.** large deviation spectrum estimation with two methods  $\varepsilon = 0.3$ .

0	0	0	0	0	0	0	0
0	0	0	0	0	0	0	0
0	0	0.462	0.462	0.000	0.000	0	0
0	0	0.000	0.000	1.041	0.883	0	0
0	0	0.000	0.000	0.000	0.833	0	0
0	0	0.674	1.000	0.000	0.000	0	0
0	0	0	0	0	0	0	0
0	0	0	0	0	0	0	0
0	0	0	0	0	0	0	0
0	0	1.000	1.095	1.136	1.136	0	0
0	0	1.462	1.195	1.534	1.407	0	0
0	0	1.000	1.534	1.534	1.512	0	0
0	0	1.095	1.381	1.557	1.348	0	0
0	0	0	0	0	0	0	0
0	0	0	0	0	0	0	0

**Table 4.** large deviation spectrum matrices with  $n = 5$

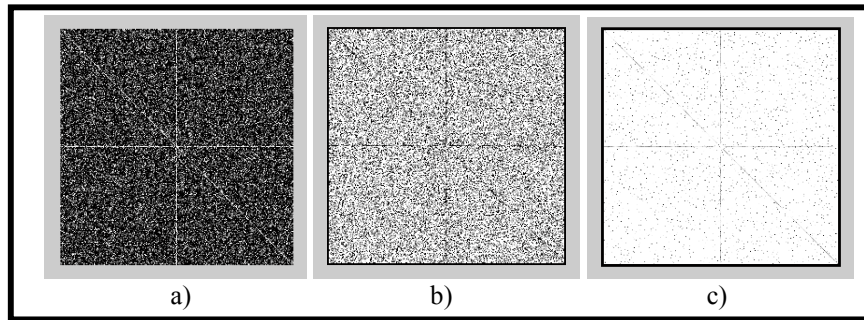
## 4. Results and experiments

In this section, we apply the two previous methods for the large deviation spectrum estimation over a synthesis image (Figure 3.) and also over an image extracted from the FracLab software (Figure 4.). Then we compare the measure that we introduce with the other measures (Figure 5, 6.).

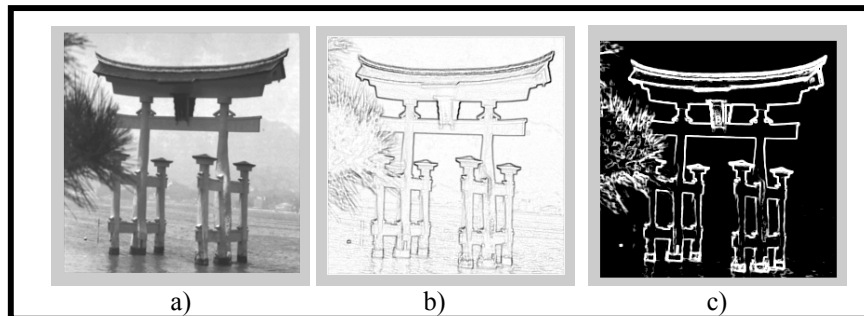
Figure 3. shows that it is interesting to introduce the gradient before applying an operator. In fact the three lines are underlined after the computation of the singularity exponents.

Figure 4. shows the singularity results with and without gradient. Singularities seem richer when using the gradient.

The more interesting comparison is shown in figure 5. and 6.. The first notable result is the display of a two dimensional spectrum. The figures show a better spectrum obtained with the gradient operator. Concerning the two methods used to compute the spectrum, we notice a better result with the second one due to  $\varepsilon$ .



**Figure 3.** a) Image representing three lines (horizontal, vertical and diagonal) with a gaussian noise ( $\sigma = 0.6$ ). b) Hölder coefficients with the iso capacity. c) Hölder coefficient computed with the gradient operator followed by the  $O = iso$  capacity here ( $n = 5$ ).



**Figure 4.** a) Original image extracted from the FracLab software [2]. b) Singularity exponents computed with the min capacity ( $n = 3$ ). c) Singularity exponents computed with the gradient operator followed by the  $O = sum$  capacity, with  $n = 3$ .

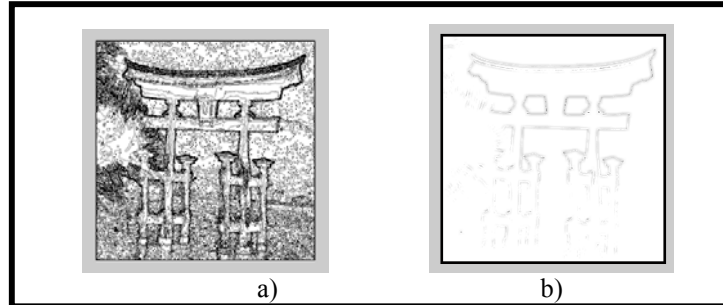


**Figure 5.** a) and b) Large deviation spectrum estimated using the first and second approach ( $\varepsilon = 0.2$ ) with  $n = 7$  from the singularity exponents of Figure 4. b).

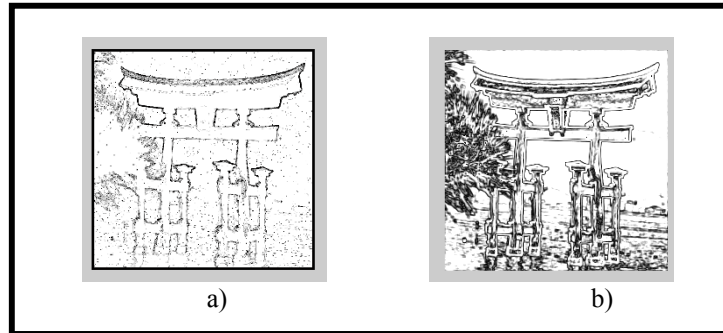


**Figure 6.** a) Large deviation spectrum estimated using the first and the second approach ( $\varepsilon = 0.2$ ) with  $n = 7$  from the singularity exponents of Figure 4. c).

## 5. Conclusion and future works

This study, deals with large deviation spectrum estimation in two dimensions. The first main conclusion is that the measure based on the gradient that we introduce is an efficient way to improve intensity variations detection. The second main conclusion is that the large deviation spectrum estimate on each pixel according to its neighbours gives a local and a global characterization of the information.

Large deviation spectrum is widely used for segmentation in the following way: computation of the singularity, computation of one dimension spectrum, segmentation of the image by integrating spectrum and singularity. Our approach allows to directly obtain a two dimension spectrum which is closed to segmentation. It will be interesting to compare the two segmentation results. In the same way, the introduction of the gradient before integrating a one dimension spectrum will be compared with two dimension spectrum.

In addition by using the second method based on the  $\varepsilon$  – value can be improve by defining a criterion of optimization which allows giving the  $\varepsilon_{opt}$  optimal value is under development.

This spectrum has been estimated using two methods based on measures built using Coquet capacity. It will be interesting for classification and segmentation purposes to combine these different spectrums (one spectrum per measure) in order to qualitatively show the interest of this study.

### Acknowledgments

The authors would like to thank the European institutions for the financing of the CESAR (Arborescent species classification) project and Guadeloupe, Martinique and Guyana regions within the “INTERREG IIIb Caribbean Space” European program.

### References

- [1] J. Lévy Véhel, Numerical Computation of Large Deviation Multifractal Spectrum, In CFIC96, Rome, 1996.
- [2] <http://www.irccyn.ec-nantes.fr/hebergement/FracLab/>
- [3] G. Parisi, U. Frisch, Turbulence and Predictability in Geophysical Fluid Dynamics and Climate Dynamics, Proc. of Int. School, 1985.
- [4] A. S. Monin, A. M. Yaglom, Statistical Fluid Mechanics, MIT Press, Cambridge, MA, vol. 2, 1975.
- [5] U. Frisch, Turbulence, Cambridge Univ. Press, Cambridge, 1995.
- [6] J. F. Muzy, E. Bacry, A. Arneodo, Phys. Rev. E 47, 875, 1993.
- [7] A. Arneodo, E. Bacry, J. F. Muzy, Physica A 213, 232, 1995.
- [8] A. Grossmann, J. Morlet, S.I.A.M. J. Math. Anal 15, 723, 1984.
- [9] A. Grossmann, J. Morlet, Mathematics and Physics, Lectures on Recent Results, L. Streit World Scientific, Singapour, 1985.
- [10] M. B. Ruskai, G. Beylkin, R. Coifman, I. Daubechies, S. Mallat, Y. Meyer, L. Raphael, Wavelets and Their Applications, Boston, 1992.
- [11] A. Turiel, N. Parga, The multi-fractal structure of contrast changes in natural images: from sharp edges to textures, Neural Computation 12, 763-793, 2000.
- [12] A. Turiel, Singularity extraction in multifractals : applications in image processing, Submitted to SIAM Journal on Applied Mathematics.
- [13] J. Lévy Véhel, R. Vojak, Multifractal analysis of Choquet capacities, Advances in applied mathematics, 1998.
- [14] J. Lévy Véhel, P. Mignot, Multifractal segmentation of images, Fractals, 371-377, 1994.
- [15] J.-P. Berroir, J. Lévy Véhel, Multifractal tools for image processing, In Proc. Scandinavian Conference on Image Analysis, vol. 1, 209-216, 1993.
- [16] H. Shekarforoush, R. Chellappa, A multi-fractal formalism for stabilization, object detection and tracking in FLIR sequences.
- [17] J. Lévy Véhel, C. Canus, Hausdorff dimension estimation and application to multifractal spectrum computation, Technical report. INRIA, 1996.